Orbital Selectivity in Scanning Tunneling Microscopy: Distance-Dependent Tunneling Process Observed in Iron Nitride

Y. Takahashi,[1] T. Miyamachi,[1,*] K. Ienaga,[1] N. Kawamura,[1,2] A. Ernst,[3] and F. Komori[1]
[1]*Institute for Solid State Physics, University of Tokyo, Kashiwa, Chiba 277-8581, Japan*
[2]*Science & Technology Research Laboratories, NHK, Setagaya, Tokyo 157-8510, Japan*
[3]*Max-Planck-Institut für Mikrostrukturphysik, Weinberg 2, 06120 Halle, Germany*
(Received 26 May 2015; revised manuscript received 3 December 2015; published 5 February 2016)

In scanning tunneling microscopy, orbital selectivity of the tunneling process can make the topographic image dependent on a tip-surface distance. We have found reproducible dependence of the images on the distance for a monatomic layer of iron nitride formed on a Cu(001) surface. Observed atomic images systematically change between a regular dot array and a dimerized structure depending on the tip-surface distance, which turns out to be the only relevant parameter in the image variation. An accompanied change in the weight of Fe-3d local density of states to a tunneling background was detected in dI/dV spectra. These have been attributed to a shift in surface orbitals detected by the tip from the d states to the s/p states with increasing the tip-surface distance, consistent with an orbital assignment from first-principles calculations.

DOI: 10.1103/PhysRevLett.116.056802

Scanning tunneling microscopy (STM) is one of the most powerful tools to investigate surface topographic and electronic structures with an atomic resolution. Surface nanostructures are often discussed based on the topographic image. However, its image contrast mainly reflects the electron tunneling processes between the STM tip and the surface orbitals at each position, i.e., local electronic states [1]. As a consequence, the image does not always correspond to the real surface morphology [2,3]. Systematic changes of the image contrast as a function of the sample-bias voltage V_s have been widely interpreted in terms of energy-dependent electronic structures [4–6]. The STM tip-surface distance d is the alternative for the image change. The strength of the STM tip-sample interaction changes at different d, which can occasionally cause the image variation [7,8]. The d-dependent image change can be expected also for the surface consisting of several orbitals with different decay length of the wave function into the vacuum, e.g., compound systems. In such systems, the image change could be induced by the shift of the dominant surface orbital contributing to the tunneling process at different d, while a certain surface state usually dominates throughout the vacuum region for elemental systems [9]. The importance of this orbital selective tunneling process on the d-dependent images was suggested for O/Ru(0001), O/Fe(001), and the rutile $TiO_2(011)-(2\times1)$ surfaces [10–13]. However, the lack of the strong experimental evidence reinforced by the solid theory still complicates achieving a common understanding of the impact of the orbital selectivity on the d-dependent imaging.

In this Letter, we advocate the importance of in-depth d-dependent STM imaging and spectroscopy to fully characterize the orbital selective tunneling as the origin of the topographic image changes. A monatomic layer of iron nitride (Fe_2N) on Cu(001) with the ferromagnetic Fe_4N stoichiometry [14,15] is chosen so as to highlight the role of the orbital selectivity. Because of the strong bonding between Fe and N atoms typical for the nitride compounds [16,17], we expect hybridization-induced non-negligible contributions of s/p orbitals relative to 3d orbitals in the local density of states (LDOS), and the robust surface structure against the tip-induced effect, which meets the purposes of this study.

We here show that the topographic image of the Fe_2N layer changed from a dimerized atomic image reflecting the atomic surface structure to a square lattice of atomic-size dots with increasing d. Corresponding systematic d dependence of the tunneling spectra implied the shift in the dominant electronic states contributing to the tunneling process. Combining with the LDOS calculations by first principles, we have attributed these to the change of the dominant orbitals detected by the STM tip from the Fe 3d states to the s/p states with increasing the tip-surface distance. The results resolve the discrepancy for the topographic images of the previous STM studies between the $p4g(2\times2)$ structure for thick films and the $c(2\times2)$ one for atomic-layer films [14,15].

Monatomic-layer iron nitrides were prepared in ultrahigh vacuum (UHV) with a base pressure of better than 1.0×10^{-10} Torr in the following process. First, a clean surface of Cu(001) was obtained by several cycles of sputtering with Ar^+ ions and subsequent annealing at 820 K. Then, N^+ ions with an energy of 0.5 keV were bombarded to the clean surface and submonolayer Fe was subsequently deposited at room temperature

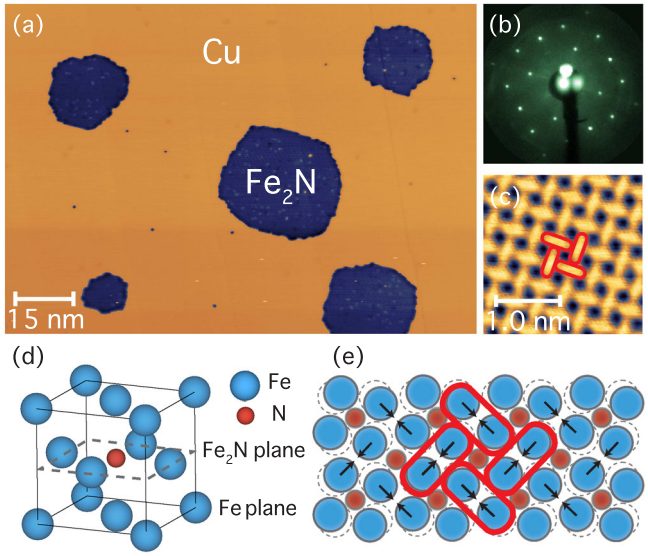

FIG. 1. (a) Large scale topographic image at $V_s = 100$ mV, $I = 5$ nA. (b) LEED pattern obtained with an incident electron energy of 100 eV. (c) Close view of a topographic image for the Fe_2N islands revealing a dimerization of Fe atoms ($V_s = 50$ mV, $I = 5$ nA). The dimerization is indicated by encirclement. (d) Crystal structure model of Fe_4N. A dotted parallelogram represents an Fe_2N plane. (e) Schema of $p4g(2 \times 2)$ surface reconstruction corresponding to the LEED pattern. From an unreconstructed coordination (dotted circles), each two of Fe atoms dimerizes in two perpendicular directions indicated by arrows.

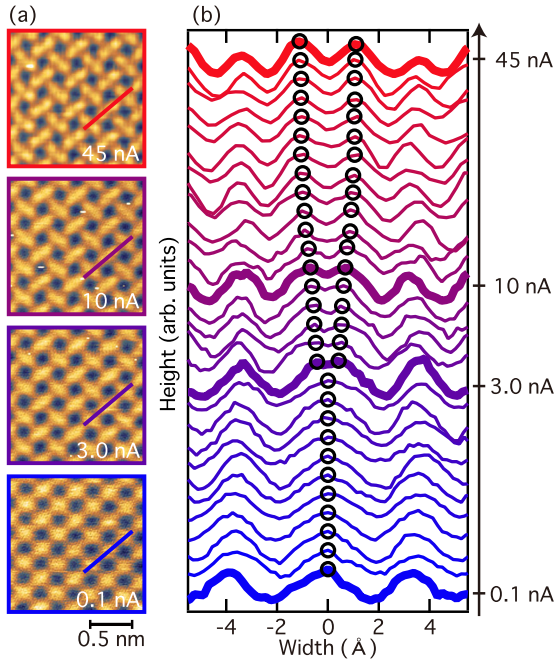

FIG. 2. Current dependence of STM images. (a) Topographic images taken at $V_s = 0.25$ V with varying I from 0.1, 3.0, 10 to 45 nA. (b) Line profiles at $V_s = 0.25$ V, measured along lines indicated in (a). From the top to the bottom, I varies as follows: 45, 40, 35, 30, 28, 25, 22, 20, 18, 15, 12, 11, 10, 9.0, 8.0, 7.0, 5.0, 3.0, 2.0, 1.0, 0.9, 0.8, 0.7, 0.6, 0.5, 0.4, 0.3, 0.2, and 0.1 nA, respectively. Empty circles indicate peak positions extracted from one Fe dimer.

(RT). After annealing at 570 K, well-ordered iron nitrides were obtained on the surface. The surface structure was confirmed by LEED at RT, and STM at 77 K. For the scanning tunneling spectroscopy, the differential conductance dI/dV was recorded using a lock-in technique with a bias-voltage modulation of 20 mV and 719 Hz.

A large-scale topographic image of the surface is shown in Fig. 1(a). Iron-nitride islands of several tens of nanometers in diameter are formed on the Cu(001) surface. A LEED pattern of the same surface shown in Fig. 1(b) exhibits the $p4g(2 \times 2)$ symmetry identical to that of the previous studies [14,15]. A close view of the STM image shows a dimerized structure as shown in Fig. 1(c), which agrees with the LEED pattern. This STM image is similar to that reported by Gallego *et al.* for the thick Fe_4N film [14]. It has been known that, irrespective of the film thickness, the topmost layer of Fe_4N films consists of an Fe_2N single layer [14,15]. In the surface layer, N atoms occupy the hollow sites of an Fe sublattice as in an Fe_4N crystal model shown in Fig. 1(d). Because of the surface reconstruction, Fe positions are different from those of an ideal Fe_2N layer of the Fe_4N crystal; the Fe atoms are dimerized in the two perpendicular directions indicated by the arrows in Fig. 1(e), which results in the decrease of the lattice constant compared to the bulk [14,15]. This surface reconstruction did occur in the films of any thickness as confirmed by LEED. Thus, it still remains unclear why the STM image of the atomic-layer films showed the $c(2 \times 2)$-like symmetry despite the $p4g(2 \times 2)$ LEED pattern [15].

To explore the origin of this discrepancy in the previous studies, we first investigated the tunneling-current (I) dependence of the STM images by fixing V_s at 0.25 V. Figure 2(a) shows a series of the images with varying I from 0.1 to 45 nA. At $I = 45$ nA, the image consists of distinct Fe dimers. With the decrease of I, the split of the Fe dimers gradually becomes ambiguous and turns into one elongated structure, similar to that reported by Gallego *et al.* [14]. Finally, at $I = 0.1$ nA, the image consists of broad dots, like that reported by Takagi *et al.* [15]. Comparing the structural model with the images for $I \geq 3.0$ nA, we specify that the dots at 0.1 nA are located at the hollow sites of the Fe sublattice with no N atom [18].

For a further grasp of the STM-image change induced by I, we extracted line profiles along the Fe dimer for various I values from 0.1 to 45 nA, as shown in Fig. 2(b). One can see that a gradual transformation from a double-peak structure to a single-peak one occurs at around $I = 3.0$ nA with decreasing I [19]. The separation between the two protrusions is almost saturated at $I \geq 20$ nA, and its maximum reaches to 2.23 Å. This length is a little smaller [20] than the reported distance between the dimerized surface Fe atoms of the Fe_2N layer, 2.83 Å of the monatomic-layer Fe_4N determined by

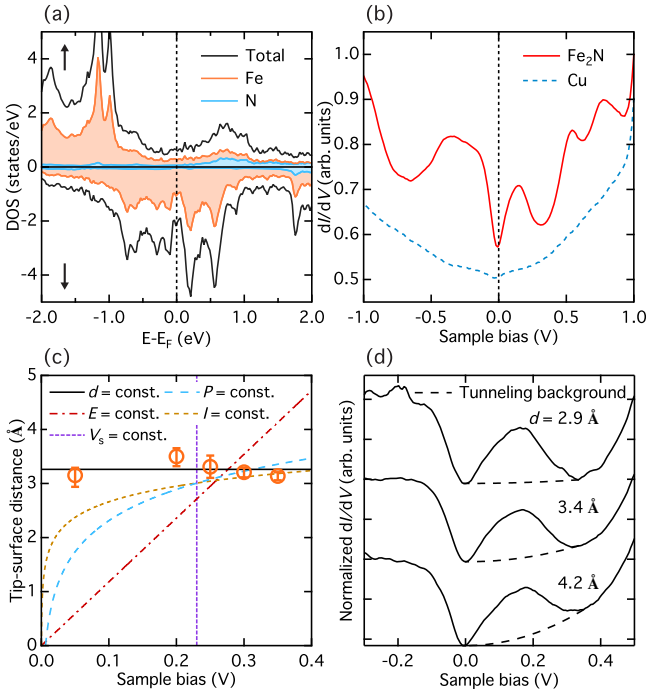

FIG. 3. (a) Spin-resolved LDOS of single-layer Fe_2N on Cu(001). Fe and N states are separately shown. (b) dI/dV spectra of Fe_2N (solid) and bare Cu (dotted). The STM tip was stabilized at $I = 30$ nA and $V_s = 1$ V. (c) Threshold d_c for the image change. Empty circles indicate parameter sets when the shift in the image from the dimerized to the dot structure occurred. Lines fitted freely to the experimental data with assuming the constant d (solid), E (dot-dashed), V_s (fine-dashed), P (rough-dashed), or I (dashed) in Eq. (1) are also indicated. (d) Distant-dependent dI/dV spectra measured at $d = 4.2$, 3.4, and 2.9 Å from the bottom to the top. Dashed curves indicate a tunneling background obtained by a Tersoff-Hamann approximation.

LEED I-V [15] and 2.73 Å of the thick Fe_4N film calculated by first principles [14].

It should be noted that the observed I dependence of the Fe-dimer image differs from what is generally expected for two adjacent protrusions in the STM observation. A protrusion in the image tends to be broader with increasing d as long as the tip state keeps overlapping the identical states at the surface. Namely, in the present case, the width of the single dot for $I < 3$ nA could be broader than the separation of the two protrusions at higher I if we assumed that the same state at the surface was detected in the entire I range. However, this is not the case in the present observations [21].

To understand the role of the electronic states for the change of STM images, we performed extensive first-principles calculations of the surface LDOS for the monatomic Fe_2N layer on Cu(001) using a self-consistent Green function method within the density functional theory (DFT), specially designed for semi-infinite layered systems [12]. Figure 3(a) shows the total, spin-resolved, and elementally resolved LDOS of the Fe_2N surface. Besides large contribution of minority spin states originating from Fe, N majority spin states also contribute to the total LDOS near the Fermi energy (E_F) at the surface. Typical dI/dV spectra recorded above the Fe_2N and Cu(001) are shown in Fig. 3(b). In contrast to the Cu spectrum with only minor features, the Fe_2N spectrum shows several peaks located at $V_s = -0.35$, -0.15, 0.17, 0.52, and 0.79 V, respectively, which well correspond to the peaks of the calculated total LDOS shown in Fig. 3(a). Note that, possibly due to the tip condition, the fine structures at the occupied states in the calculation are not so obvious in the experimental dI/dV spectrum. Thus, hereafter we focus on the unoccupied states (positive sample bias) near the E_F.

In the STM measurement, local atomic structures and/or electronic properties of the surface can be modified by the experimental parameters such as I, V_s, d, the local Joule heating $P = V_s \times I$, and the electric field $E = V_s/d$ [22]. To elucidate which parameter is crucial to induce the transformation of the STM image in the present study, we have taken the images in various combinations of I and V_s. Here, we determine I_c and d_c, which denote the critical tunneling current and tip-sample distance that the image transforms from the dimerized to the dot structure, respectively. The d_c was evaluated from I_c at each V_s by applying Simmons'rule [23]

$$d_c = -\frac{\hbar}{2\sqrt{2m\Phi}} \ln\left(\frac{R_0 I_c}{V_s}\right), \quad (1)$$

where m is the electron mass, Φ an average work function of the tip and the sample, and R_0 the resistance for a single-atomic point contact of 12.9 kΩ [24]. An average Φ value of 5.5 eV, obtained from the fitting of several experimental I-d curves is used in the evaluation [25]. Figure 3(c) shows a plot of d_c as a function of V_s (empty circles). The nearly constant d_c values of 3.3 Å (solid line) are found, suggesting that I_c increases (decreases) at higher (lower) V_s, and the image change is entirely caused by d. None of E, V_s, P, and I can be a threshold for the image change. Therefore, we can conclude that the observed image change is triggered by the tip-surface distance [26].

It has been known that the decay length of the wave function strongly depends on an orbital character; i.e., the $3d$ states decay into the vacuum faster than the s/p states [27]. The different decay lengths between the d and s/p states were previously investigated and confirmed in terms of the spin polarization [28,29]. Thus, the states detected by the tip with smaller distance could have more Fe $3d$ character.

To confirm this, we measured dI/dV spectra with various d values as shown in Fig. 3(d). Here, the tip was fixed at $V_s = 0.1$ V, and all the spectra are normalized to the intensity at $V_s = -0.1$ V. Note that the corresponding STM images at $d = 2.9$, 3.4, and 4.2 Å consist of the distinct, blurred, dimerized structures and the dot structure, respectively. At $d = 2.9$ Å, the background contribution is

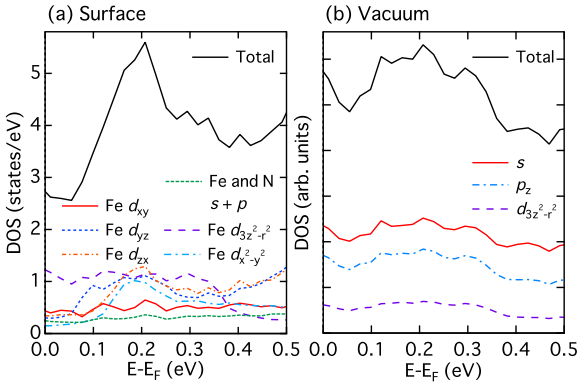

FIG. 4. Total and orbital-resolved LDOS of (a) surface and (b) vacuum (4 Å above the surface) layers. The states with negligible intensity in this energy range are not shown here. In the vacuum layer, LDOS cannot be separated into each atomic component due to a strong orbital mixing between Fe and N.

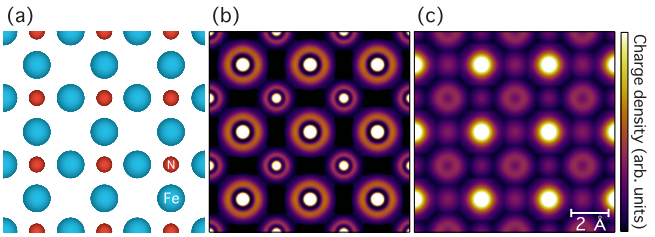

FIG. 5. Charge distributions calculated at different distances. (a) Unreconstructed $c(2\times 2)$ surface model used for the calculation. Large (small) spheres correspond to the surface Fe (N) atoms. (b,c) Charge distribution at $d = 1.8$ (b) and $d = 6.5$ Å (c).

small and the peak around 0.2 V is mainly attributed to the Fe $3d$ state, in comparison with the theoretical calculations [see Fig. 3(a) and the detailed orbital assignment discussed below]. However, one can clearly see that the contribution of an integrated background signal monotonically increases as the tip becomes far. It should be noted that an exponential background signal is mainly due to the tunneling processes between the tip states and the sample s/p states [27,30]. Therefore, a series of the d-dependent dI/dV spectra well supports our interpretation of the observed d-dependent change of the STM image. Namely, at short d, the tunneling process through the Fe $3d$ states dominates that through the s/p states, and it results in the STM image of the dimerized structure.

We have further studied the decay of orbital-resolved LDOS into the vacuum by first-principles calculations to understand the tunneling process in detail. In Figs. 4(a) and 4(b), we extract dominant orbitals contributing to the total LDOS near the E_F. At the surface, the LDOS mainly consists of the Fe $3d$ states and the s/p states are minute as shown in Fig. 4(a). It means that, at a short tip-surface distance, the possible states dominantly detected by the STM tip are $3d_{3z^2-r^2}$, $3d_{zx}$, and $3d_{yz}$. Another intriguing is that among $3d$ states, the d_{xy} state shows no clear LDOS around $E - E_F = 0.2$ eV. This indicates a strong hybridization between Fe and N atoms, which leads to delocalization of the d_{xy} state while the other $3d$ states relatively remain localized.

The situation drastically changed in the vacuum layer 4 Å above the surface. In Fig. 4(b), one can see that the contributions of isotropic s and out-of-plane-oriented p_z overwhelm those of $3d$ except for $3d_{3z^2-r^2}$. This is clearly due to the longer decay lengths of the s/p states than the d states. Such large s/p contributions relative to the $3d$ ones and thus the tip-surface distance dependence of the STM image have not been expected in elemental $3d$ systems, where the surface states mainly of $d_{3z^2-r^2}$ character slowly decay into the vacuum [9]. The considerable enhancement of the s/p contribution in the present case is caused by strong hybridization of N s/p states with Fe s, p, d states, which is characteristic of compound systems.

Finally, we confirm how this shift in the s/p and d contributions at different distances shows up in a spatial distribution of the charge density using DFT. Figure 5 shows the calculated charge distributions of states at the energy $E = E_F + 0.25$ eV, corresponding to our experimental V_s of 0.25 V. It should be noted that an energy resolved charge distribution can be associated with STM topographic images within the Tersoff-Hamann model [1]. An unreconstructed $c(2\times 2)$ surface shown in Fig. 5(a) was used in the calculation for simplicity, instead of the reconstructed $p4g(2\times 2)$ one. Thus, obtained charge distributions at $d = 1.8$ and 6.5 Å are shown in Figs. 5(b) and 5(c), respectively [31]. At a shorter distance of 1.8 Å, the charge intensity is high on top of the Fe atoms, because of a large contribution of the Fe $3d$ states. This is consistent with the fact that the surface Fe atoms were distinctly imaged at higher I's [see Fig. 2(a)]. In the case of $d = 6.5$ Å, in contrast, the intensity maxima locate above the hollow site of the Fe sublattice without N atoms. This originates from the dominance of states with s/p characters at larger distances, and well reproduces the experimental I dependence of the STM images.

In summary, we have performed the comprehensive STM work to elucidate the origin of the image changes for the monatomic-layer iron nitride on Cu(001). Systematic d-dependent STM imaging and spectroscopy reveal that the observed image change is attributed to the orbital-dependent decay length of the wave function at the surface. The validity of the experimental results is confirmed by the first-principles calculations, which successfully reproduce that the STM image is dominated by the Fe $3d$ states at short distance whereas by the s/p states at long distance. Since the orbital-selective tunneling process is inherent in any STM measurements, the atomic morphology based on the topographic image should be carefully discussed, especially in the compound systems.

This work was partly supported by the JSPS Grant-in-Aid for Young Scientists (B), Grant No. 26790004, for

Scientific Research (B), Grant No. 26287061, and the Hoso Bunka Foundation. Y. T. was supported by the Grant-in-Aid for JSPS Fellows and the Program for Leading Graduate Schools (MERIT). A. E. acknowledges funding by the German Research Foundation (DFG Grant No. ER 340/4-1).

*toshio.miyamachi@issp.u-tokyo.ac.jp

[1] J. Tersoff and D. R. Hamann, Phys. Rev. B **31**, 805 (1985).
[2] T. Choi, C. D. Ruggiero, and J. A. Gupta, Phys. Rev. B **78**, 035430 (2008).
[3] Y. Nakamura, Y. Kondo, J. Nakamura, and S. Watanabe, Phys. Rev. Lett. **87**, 156102 (2001).
[4] S. Heinze, S. Blügel, R. Pascal, M. Bode, and R. Wiesendanger, Phys. Rev. B **58**, 16432 (1998).
[5] E. J. van Loenen, J. E. Demuth, R. M. Tromp, and R. J. Hamers, Phys. Rev. Lett. **58**, 373 (1987).
[6] G. M. Rutter, N. P. Guisinger, J. N. Crain, E. A. A. Jarvis, M. D. Stiles, T. Li, P. N. First, and J. A. Stroscio, Phys. Rev. B **76**, 235416 (2007).
[7] G. Doyen, D. Drakova, J. V. Barth, R. Schuster, T. Gritsch, R. J. Behm, and G. Ertl, Phys. Rev. B **48**, 1738 (1993).
[8] M. Böhringer, W.-D. Schneider, R. Berndt, K. Glöckler, M. Sokolowski, and E. Umbach, Phys. Rev. B **57**, 4081 (1998).
[9] J. A. Stroscio, D. T. Pierce, A. Davies, R. J. Celotta, and M. Weinert, Phys. Rev. Lett. **75**, 2960 (1995).
[10] F. Calleja, A. Arnau, J. J. Hinarejos, A. L. Vázquez de Parga, W. A. Hofer, P. M. Echenique, and R. Miranda, Phys. Rev. Lett. **92**, 206101 (2004).
[11] A. Picone, G. Fratesi, A. Brambilla, P. Sessi, F. Donati, S. Achilli, L. Maini, M. I. Trioni, C. S. Casari, M. Passoni, A. Li Bassi, M. Finazzi, L. Duò, and F. Ciccacci, Phys. Rev. B **81**, 115450 (2010).
[12] A. Tange, C. L. Gao, B. Y. Yavorsky, I. V. Maznichenko, C. Etz, A. Ernst, W. Hergert, I. Mertig, W. Wulfhekel, and J. Kirschner, Phys. Rev. B **81**, 195410 (2010).
[13] T. Woolcot, G. Teobaldi, C. L. Pang, N. S. Beglitis, A. J. Fisher, W. A. Hofer, and G. Thornton, Phys. Rev. Lett. **109**, 156105 (2012).
[14] J. M. Gallego, D. O. Boerma, R. Miranda, and F. Ynduráin, Phys. Rev. Lett. **95**, 136102 (2005).
[15] Y. Takagi, K. Isami, I. Yamamoto, T. Nakagawa, and T. Yokoyama, Phys. Rev. B **81**, 035422 (2010).
[16] S. Driver and D. Woodruff, Surf. Sci. **442**, 1 (1999).
[17] F. Komori, S. Ohno, and K. Nakatsuji, Prog. Surf. Sci. **77**, 1 (2004).
[18] See also Fig. 5 and related discussion on the charge distributions calculated at different distances.
[19] This threshold slightly changes depending on the tip condition.
[20] This could be attributed to the difference between an exact atomic position and a projected LDOS distribution of the Fe dimer at each set point.
[21] See Supplemental Material at http://link.aps.org/supplemental/10.1103/PhysRevLett.116.056802 for a numerical simulation of simple broadening of the charge density.
[22] L. Gerhard, T. K. Yamada, T. Balashov, A. F. Takacs, R. J. H. Wesselink, M. Dane, M. Fechner, S. Ostanin, A. Ernst, I. Mertig, and W. Wulfhekel, Nat. Nanotechnol. **5**, 792 (2010).
[23] J. G. Simmons, J. Appl. Phys. **34**, 1793 (1963).
[24] B. J. van Wees, H. van Houten, C. W. J. Beenakker, J. G. Williamson, L. P. Kouwenhoven, D. van der Marel, and C. T. Foxon, Phys. Rev. Lett. **60**, 848 (1988).
[25] See Supplemental Material at http://link.aps.org/supplemental/10.1103/PhysRevLett.116.056802 for the nearly constant Φ values with respect to the tip-surface distance.
[26] The observed LEED pattern agrees with the STM image at short d. Therefore, the tip-sample interaction is excluded as the origin of the image change in the present case.
[27] C. Julian Chen, *Introduction to Scanning Tunneling Microscopy* (Oxford University Press, New York, 1993).
[28] S. F. Alvarado, Phys. Rev. Lett. **75**, 513 (1995).
[29] M. Eltschka, B. Jäck, M. Assig, O. V. Kondrashov, M. A. Skvortsov, M. Etzkorn, C. R. Ast, and K. Kern, Nano Lett. **14**, 7171 (2014).
[30] V. A. Ukraintsev, Phys. Rev. B **53**, 11176 (1996).
[31] Note that the distances of the calculation cannot be directly compared the experiments since DFT has less accuracy for reproducing the surface excess charge.